Supplement for "MAX-DOAS measurements of HONO slant column densities during the MAD-CAT Campaign: inter-comparison and sensitivity studies on spectral analysis settings"

Yang Wang[1,2], Steffen Beirle[1], Francois Hendrick[3], Andreas Hilboll[4,5], Junli Jin[6,7], Aleksandra A. Kyuberis[8], Johannes Lampel[9,1], Ang Li[2], Yuhan Luo[2], Lorenzo Lodi[10], Jianzhong Ma[6], Monica Navarro[11], Ivan Ortega[12], Enno Peters[4], Oleg L. Polyansky[10,8], Julia Remmers[1], Andreas Richter[4], Olga Puentedura Rodriguez[11], Michel Van Roozendael[3], André Seyler[4], Jonathan Tennyson[10], Rainer Volkamer[12], Pinhua Xie[2,13], Nikolai F. Zobov[8] and Thomas Wagner[1]

[1] Max Planck Institute for Chemistry, Mainz, Germany
[2] Anhui Institute of Optics and Fine Mechanics, Key laboratory of Environmental Optics and Technology, Chinese Academy of Sciences, Hefei, 230031, China
[3] Belgian Institute for Space Aeronomy – BIRA-IASB, Brussels, Belgium
[4] Institute of Environmental Physics, University of Bremen, Bremen, Germany
[5] Center for Marine Environmental Sciences (MARUM), University of Bremen, Bremen, Germany
[6] Chinese Academy of Meteorological Sciences, Beijing, China
[7] CMA Meteorological Observation Centre, Beijing, China
[8] Institute of Applied Physics, Russian Academy of Sciences, Nizhny Novgorod, Russia
[9] Institute of Environmental Physics, University of Heidelberg, Heidelberg, Germany
[10] Department of Physics and Astronomy, University College London, Gower St, London WC1E 6BT, UK
[11] Area de Investigación e Instrumentación Atmosférica, INTA, Torrejón de Ardoz, Spain
[12] Department of Chemistry and Biochemistry, University of Colorado, Boulder, CO, USA
[13] CAS Center for Excellence in Urban Atmospheric Environment, Institute of Urban Environment, Chinese Academy of Sciences, Xiamen, 361021, China

Correspondence to: Yang Wang (y.wang@mpic.de); Ang Li (angli@aiofm.ac.cn)

1 Synthetic spectra

All simulations have been conducted with the radiative transfer model (RTM) SCIATRAN (Rozanov et al., 2014), version 3.6.0 (03 Dec 2015). SCIATRAN has been operated in Raman mode to simulate intensities of scattered and transmitted sunlight in Mainz, Germany (49.99°N, 8.23°E), including the effect of rotational Raman scattering in the Earth's atmosphere. The most important parameters of model runs are given in Table S1. The scalar radiative transfer problem has been solved in a pseudo-spherical atmosphere (i.e., the solar beam is treated in spherical geometry, while the scattered or reflected beam is treated in plane-parallel geometry) using the discrete ordinate method. The simulations have been conducted with 0.01nm spectral sampling, and rotational Raman lines have been calculated using the forward-adjoint approach and binned to the 0.01nm wavelength grid. Contribution from vibrational Raman scattering was not simulated, as we assume that its contribution is comparably small and most of it will be automatically compensated for in measured data by the additional intensity offset correction in DOAS fits (Lampel et al., 2015). Absorption by the trace gases ozone (O_3), nitrogen dioxide (NO_2), formaldehyde (HCHO), bromine oxide (BrO), nitrous acid (HONO), glyoxal (CHOCHO), by water vapour (H_2O (vap)), and by the O_2–O_2 collision complex (O_4) has been considered; the respective cross-section references are given in Table S2. Aerosols were assumed to be mostly scattering, having an optical depth (AOD) of 0.135, an asymmetry factor of 0.68, and a single scattering albedo (SSA) of 0.94. The atmospheric scenario is set to represent the conditions during the MAD-CAT campaign, which is an urban

northern mid-latitude summer setting. Atmospheric temperature and pressure profiles have been derived from an averaged surface temperature of 292 K and a surface pressure of 1002 hPa, assuming a lapse rate of 0.0645 K km^{-1}. Lower tropospheric vertical profiles of NO_2, HCHO, CHOCHO, and aerosol extinction were acquired from the measurements by the CU AMAX-DOAS instrument during the CalNex campaign over Los Angeles (Baidar et al., 2013). The trace gas vertical profiles for the mid- and upper troposphere and the stratosphere, as well as the O_3 profile are taken from a 2D climatology for the month of June at 55°N, derived from the Bremen 3D CTM (Sinnhuber et al., 2002 and 2003). The H_2O(vap) vertical profile was estimated based on near-surface air temperature, air pressure, and humidity observed by the IPA weather station in Mainz/Germany during the MAD-CAT campaign. The BrO vertical profile is a northern mid-latitude summer (45°N, July, 35° solar zenith angle, 325DU O_3 column density) climatology derived from the BASCOE model (Theys et al., 2009). The simulated spectra have been down-sampled to 0.05nm resolution before being convoluted with a Gaussian (FWHM 0.5nm) to simulate the instrument response function. The simulated measurement geometries reflect one full day of actual MAX-DOAS measurements during the MAD-CAT campaign. The elevation angles 1°, 2°, 3°, 4°, 5°, 6°, 8°, 10°, 15°, 30°, and 90° were simulated, with an assumed viewing azimuth angle of 51°. The solar geometries are detailed in Table S1

Table S1 The parameters for the simulations of the synthetic spectra.

RTM	SCIATRAN 3.6.0 in a pseudo-spherical atmosphere		
Simulation sampling	0.01 nm		
Absorption species	O_3, NO_2, HCHO, CHOCHO, HONO, BrO, O_4, water vapor (HITRAN for Version 1, and POKAZATEL for Version 2)		
Assumed instrument Sampling	0.05 nm		
instrumental function	a Gaussian of 0.5 nm FWHM		
Aerosols	AOD of 0.135, Asymmetry factor of 0.68, Single scattering albedo of 0.94		
Random noise	1. Without random noise 2. With a Gaussian noise at a SNR of 3000		
Instrument geometry	Elevation angle (1°, 2°, 3°, 4°, 5°, 6°, 8°, 10°, 15°, 30°, 90°); azimuth angle (51°)		
Raman scattering	Rotational Raman scattering		
Sun geometry	UTC (h)	SZA (°)	SAA (°)
	4.48	85	64
	4.96	80	69
	6.08	70	81
	7.21	60	94
	8.14	50	106
	9.38	40	125
	11.20	30	166
	12.14	30	194
	13.99	40	235
	15.25	50	254
	16.20	60	266
	17.34	70	279
	18.47	80	291
	18.96	85	296
	19.64	88	303
	20.21	90	309

Table S2 Absorption cross-sections used in the simulation of the synthetic spectra.

Trace gas	**Reference**
O_4	Thalman and Volkamer (2013)
O_3	Serdyuchenko et al. (2014) and Gorshelev et al. (2014)
NO_2	Vandaele et al. (1998)
HCHO	Meller and Moortgat (2000)
BrO	Fleischmann et al. (2004)
HONO	Stutz et al. (2000)
CHOCHO	Volkamer et al. (2005)
H_2O (vap)	Rothman et al., 2013 for Version 1 and Polyansky et al., 2016 (scaled by a factor of 2.6 in the UV range) for Version 2

Figures:

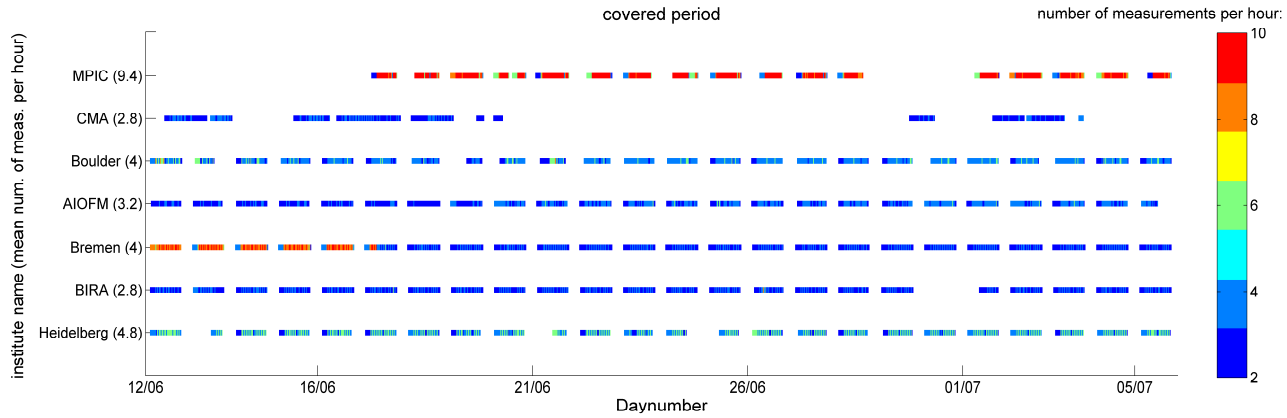

Figure S1: Time coverage of the different instruments during the period used for the HONO comparisons. The color map indicates the number of the elevation sequences per hour. The mean values for each instrument are given in brackets at the y-axis.

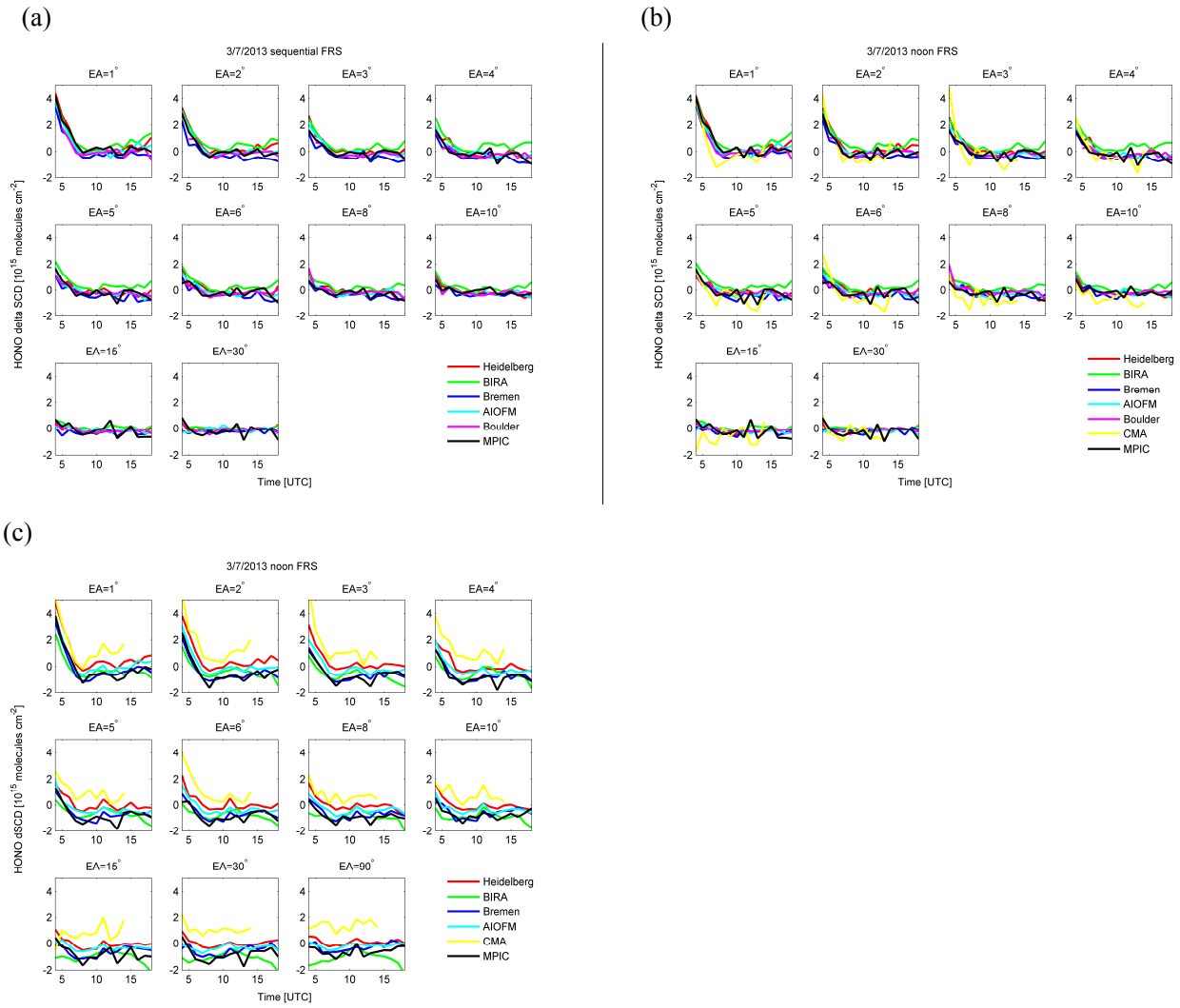

Figure S2: Time series of the hourly averaged values of HONO delta SCDs using a sequential FRS (a) and a daily noon FRS (b) as well as the HONO dSCDs with a daily noon FRS (c) for individual elevation angles and instruments on 3 July 2013.

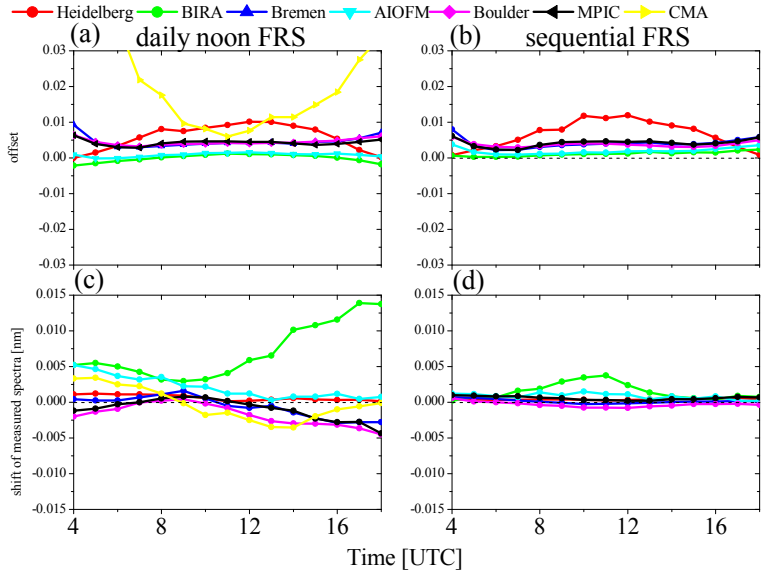

Figure S3: For the spectra measured at 1° elevation angle by individual instruments, Top: Averaged diurnal variations of the intensity offset derived from DOAS fits with either a daily noon FRS (a) or a sequential FRS (b). Bottom: Averaged diurnal variations of the wavelength shift derived from DOAS fits with either a daily noon (c) or a sequential FRS (d).

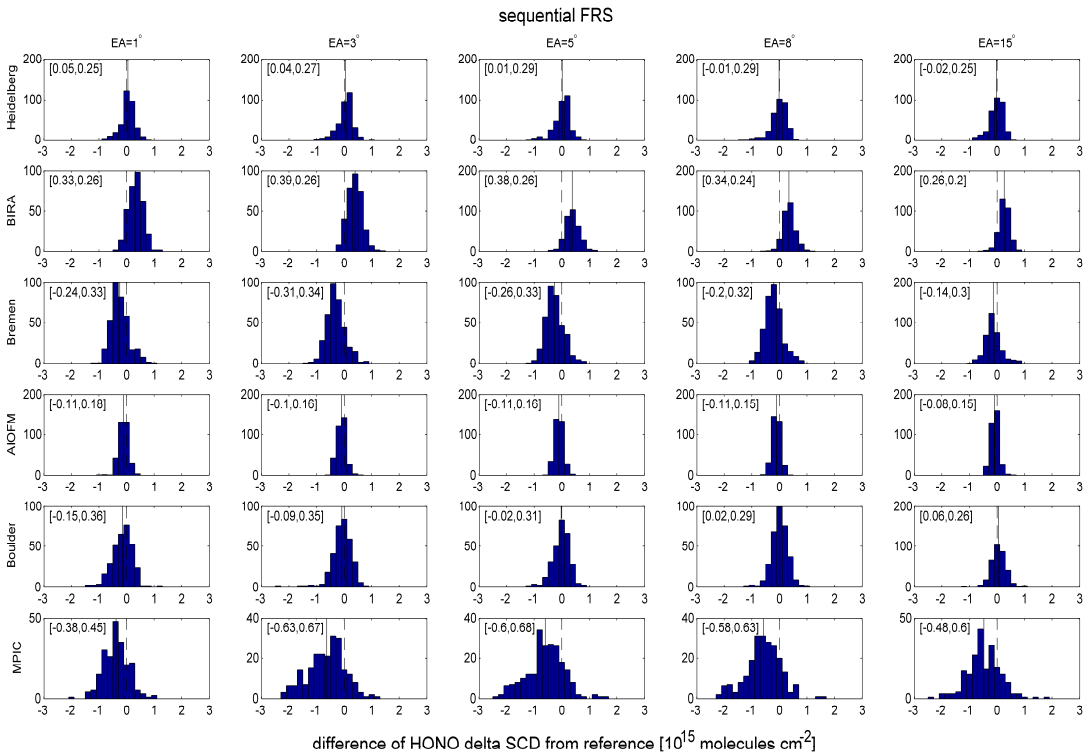

Figure S4: Histograms of absolute differences of HONO delta SCDs for each instrument with respect to the reference values during the whole comparison period and for different elevation angles; The mean differences and standard deviations are given in the square brackets in each subfigure. The dashed lines and vertical lines indicate the x-axis values of zero and the mean differences in each subfigure.

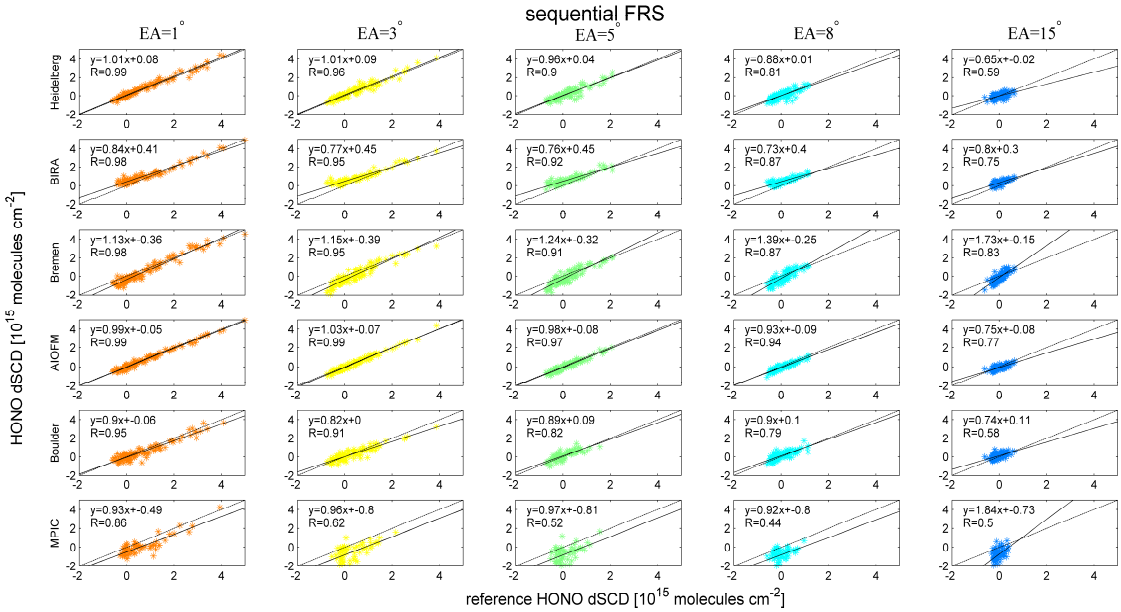

Figure S5: Linear regressions of HONO delta SCDs derived for the different instruments against the reference values for different elevation angles; the correlation coefficients and the results of the linear regressions are displayed in individual subfigures. The solid and dashed vertical lines in each subfigure indicate the fitted regression lines and the 1:1 lines.

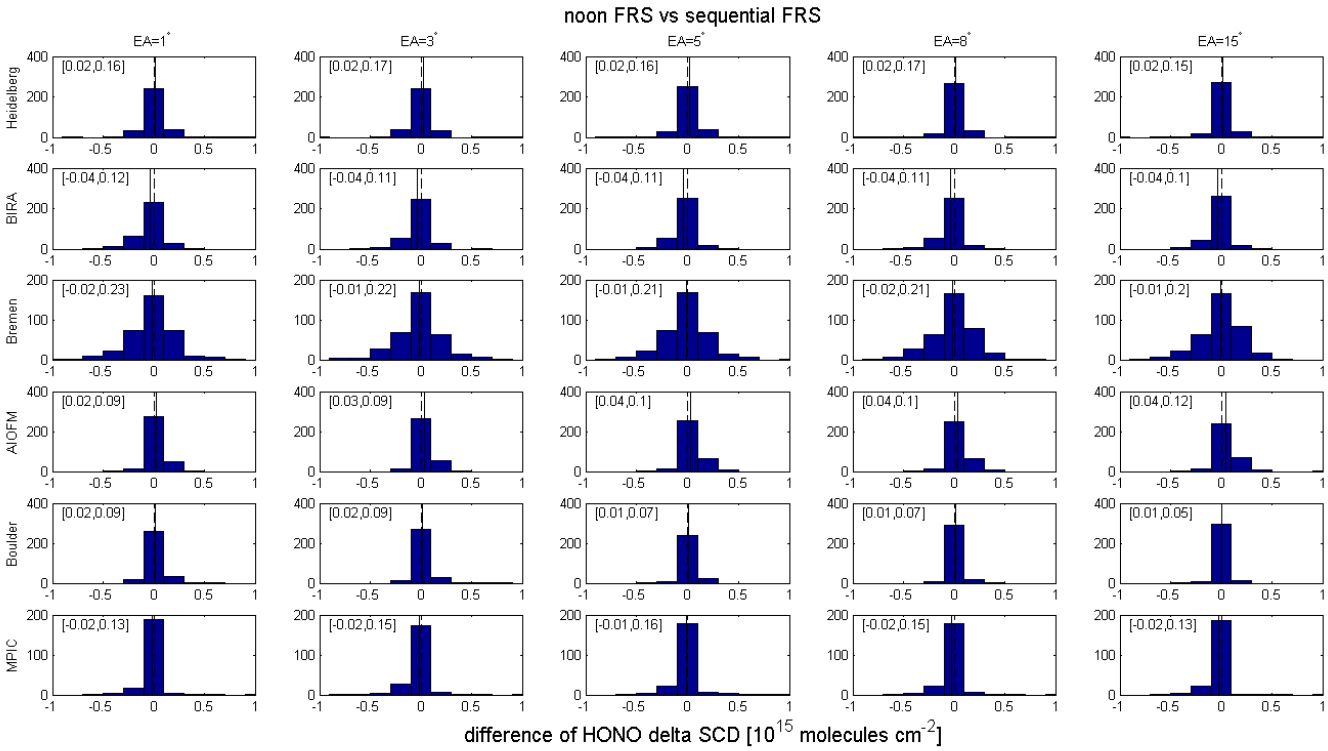

Figure S6: Histograms of absolute differences of the HONO delta SCDs for each instrument with respect to the results with a daily noon FRS and with a sequential FRS for the whole comparison period for the different elevation angles; the values in the square brackets in each subfigure represent the corresponding mean differences and standard deviations.

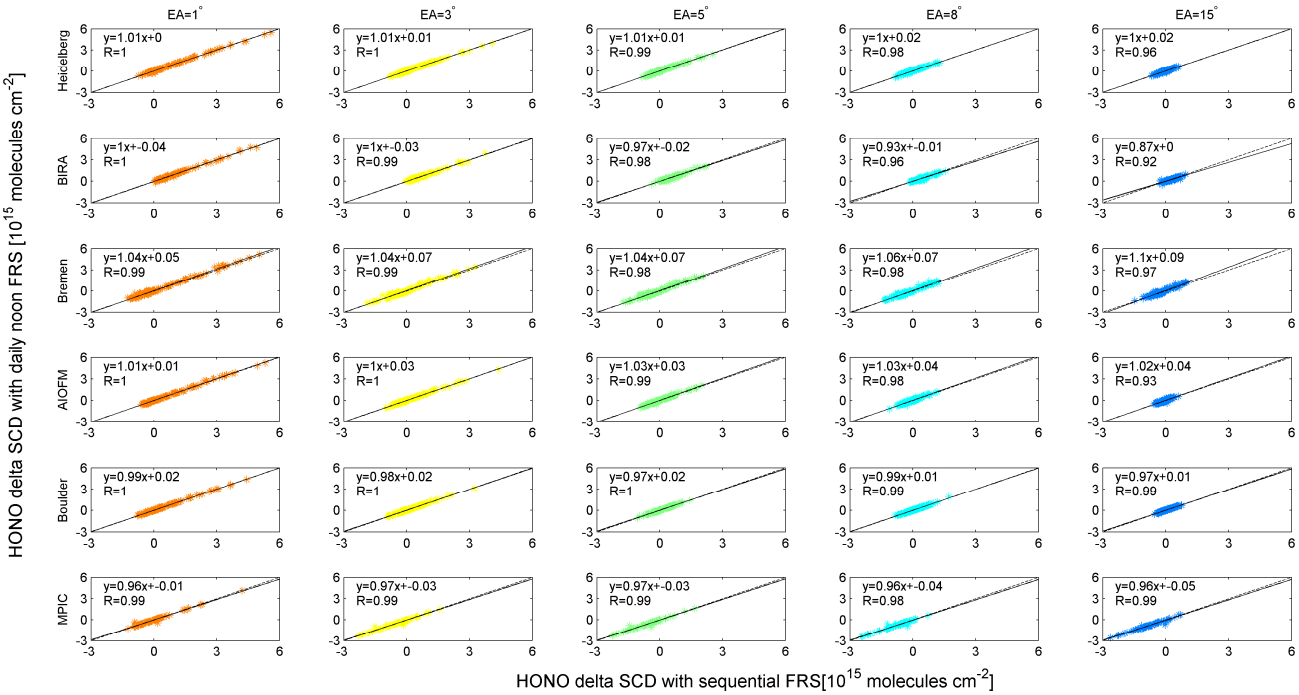

Figure S7: Linear regressions of HONO delta SCDs derived for the different instruments using a daily noon FRS against those with a sequential FRS for the different elevation angles; the correlation coefficients and the results of linear regressions are displayed in the individual subfigures.

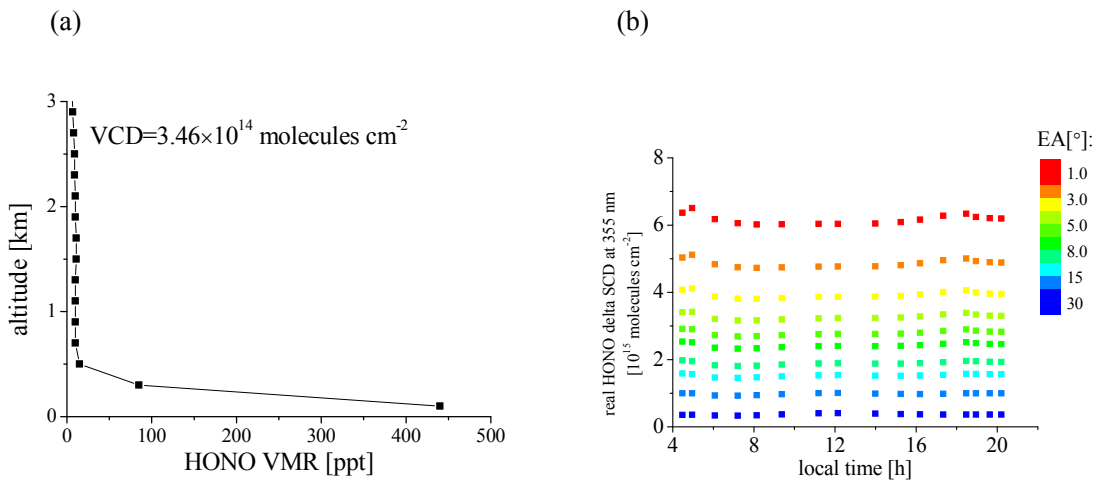

Figure S8: (a) Profile of the HONO VMR used for the generation of the synthetic spectra; (b) real HONO delta SCDs at 355 nm corresponding to the synthetic spectra (the color map indicates the elevation angles).

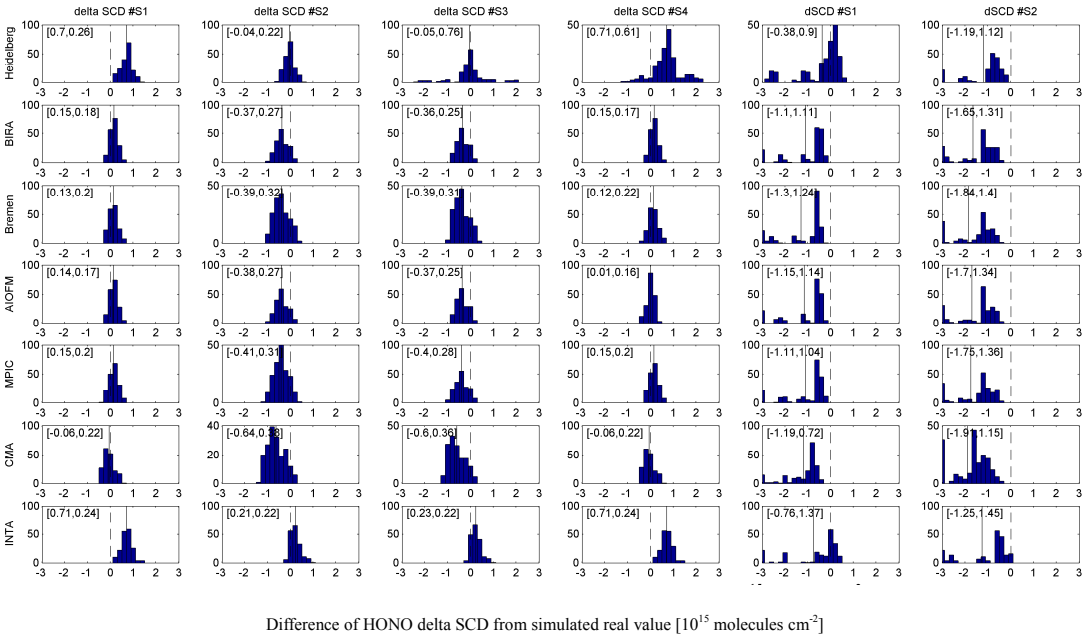

Figure S9: Histograms of absolute differences of the HONO delta SCDs or dSCDs for the different groups with respect to the real values (for the V1 synthetic spectra) for different DOAS fit settings (see Table 3). The mean differences and standard deviations for each histogram are given in square brackets in each subfigure. The dashed lines and vertical lines indicate zero and the mean differences in each subfigure.

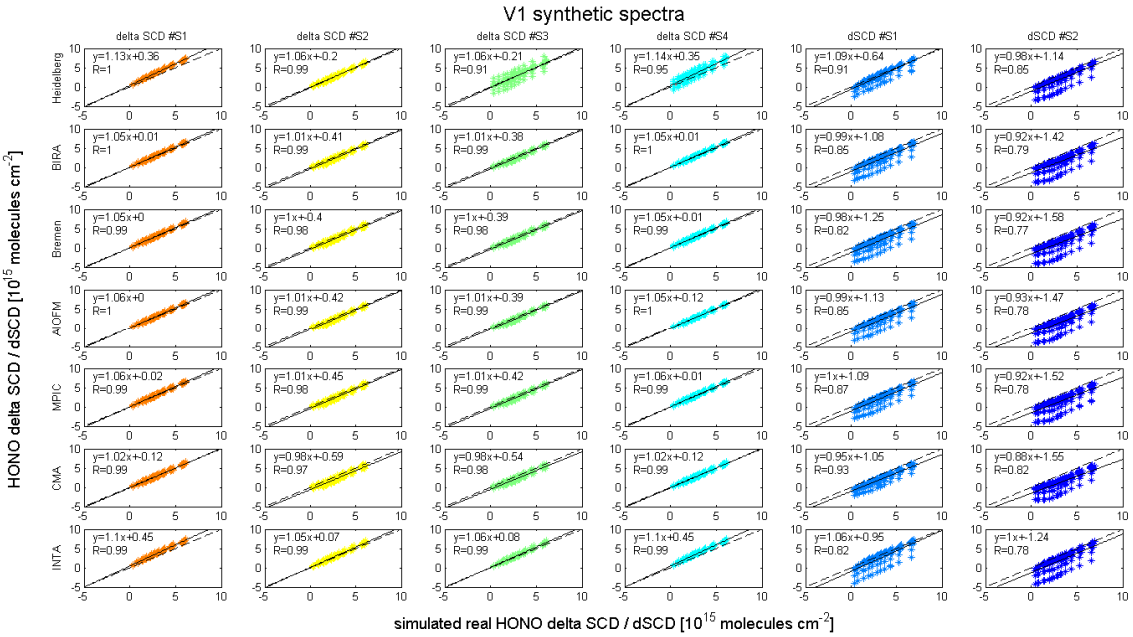

Figure S10: Linear regressions of HONO delta SCDs or dSCDs derived by the different groups against the real values for the V1 synthetic spectra and for the different DOAS fit settings (see Table 3); the correlation coefficients and the results of the linear regressions are displayed in individual subfigures. The solid and dashed lines in each subfigure indicate the linear regressions and the 1:1 lines.

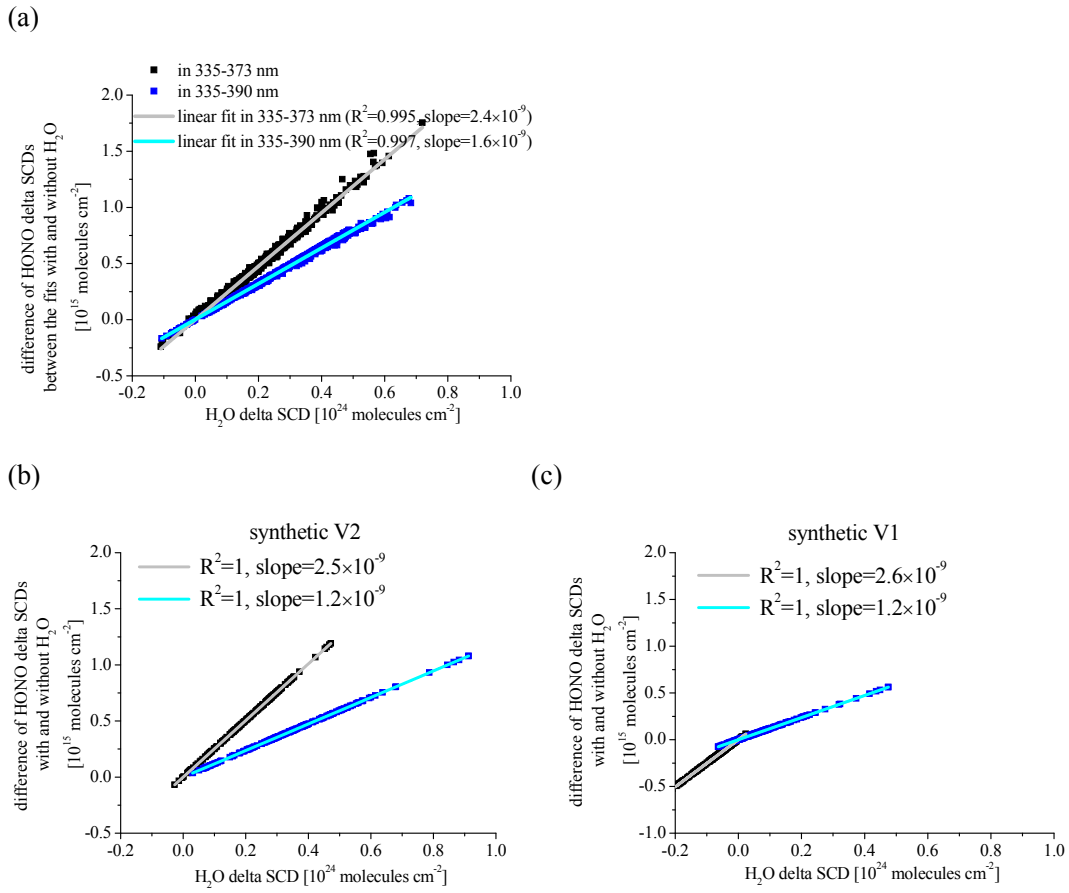

Figure S11: (a) Scatter plots of differences of the HONO delta SCDs from fits with and without the POKAZATEL H_2O cross section versus the retrieved H_2O delta SCDs for measured spectra by the AIOFM instrument on the two selected days (16 and 18 June, 2013). The correlation coefficients from the linear regressions are given in the figure; the fits are done in the spectral ranges of 335 – 373 nm (black dots and grey line) and 335 – 390 nm (blue dots and light blue line), respectively. (b) same as (a), but for the V2 synthetic spectra. (c) same as (a), but for the V1 synthetic spectra.

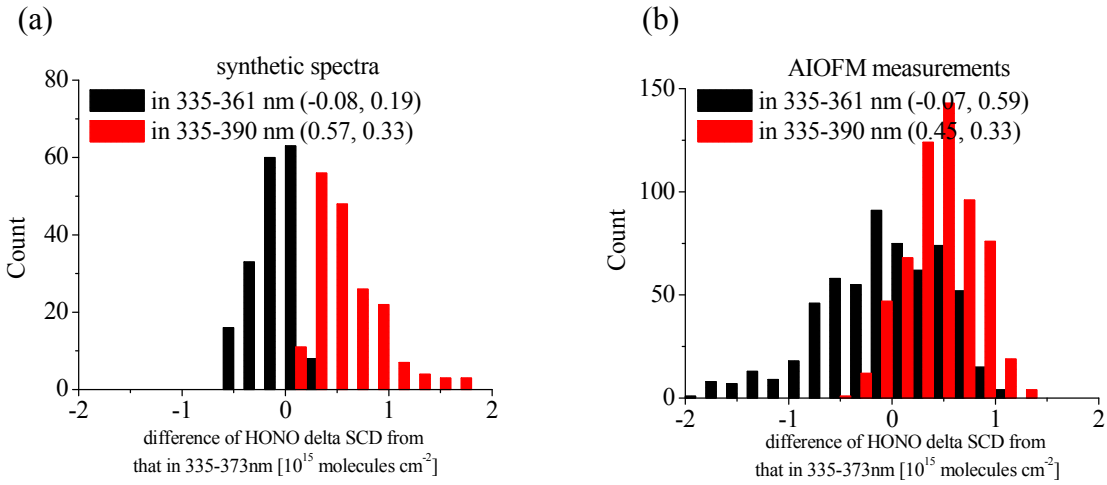

Figure S12: (a) Histograms of differences of the HONO delta SCDs retrieved in the two alternative spectral ranges (335-361 nm and 335-390 nm) with respect to the spectral range of the basic settings (335-373 nm) for the V1 synthetic spectra; (b) same as (a) but for the selected measurements by the AIOFM instrument on two days of 16 and 18 June, 2013. The mean differences and standard deviations are given in the round brackets in each subfigure

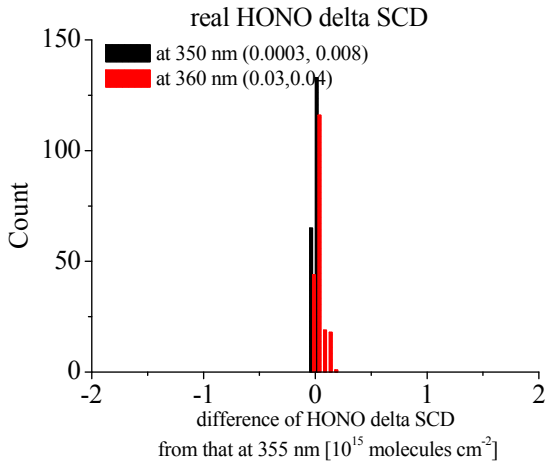

Figure S13 Histograms of differences of real HONO delta SCDs at 350 nm and 360 nm from those at 373 nm for the V1 synthetic spectra. The mean differences and standard deviations are given in the round brackets.

(a)

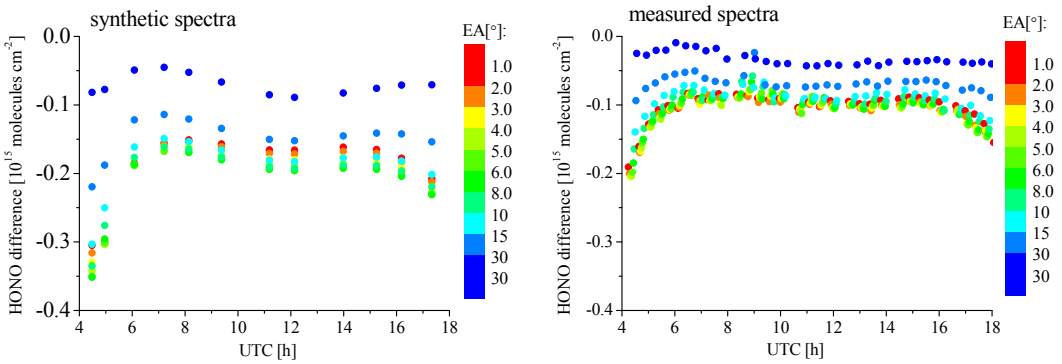

(b)

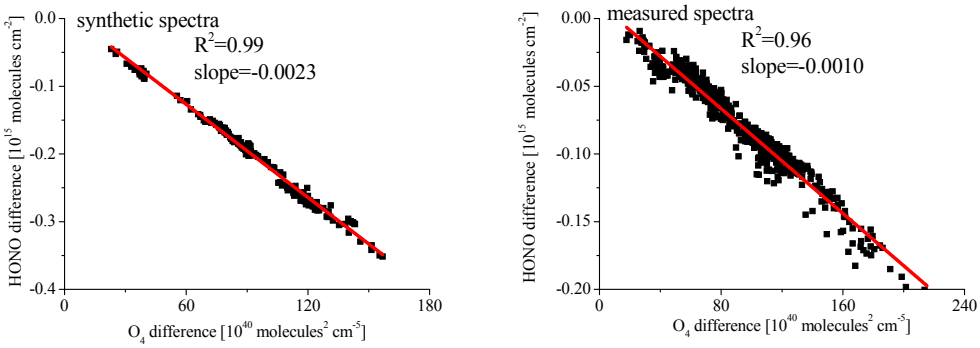

Figure S14: (a): Differences of HONO delta SCDs derived from spectral analyses with either the Thalman or the Hermans O_4 cross section for V1 synthetic spectra (left) and measured spectra (right). (b): Scatter plots of the differences of the HONO delta SCDs versus those of the O_4 delta SCDs for using either the Thalman or the Hermans O_4 cross section in the fit (left: V1 synthetic spectra; right: selected spectra from the AIOFM instrument on 16 June).

(a)

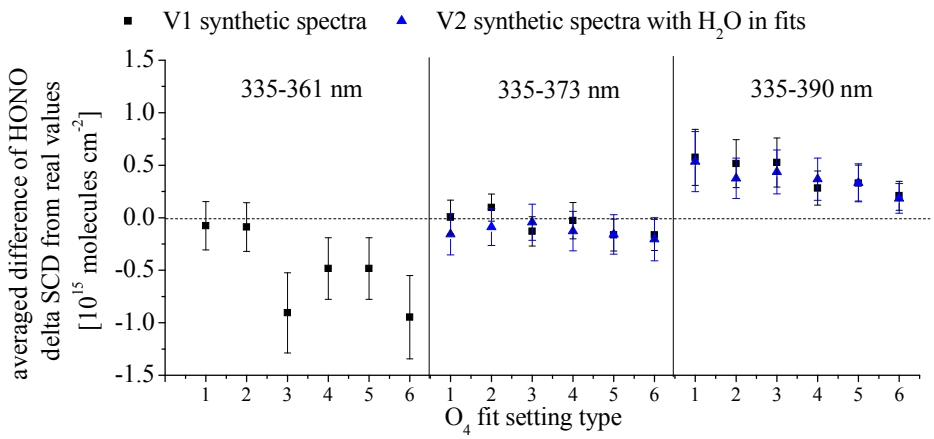

(b)

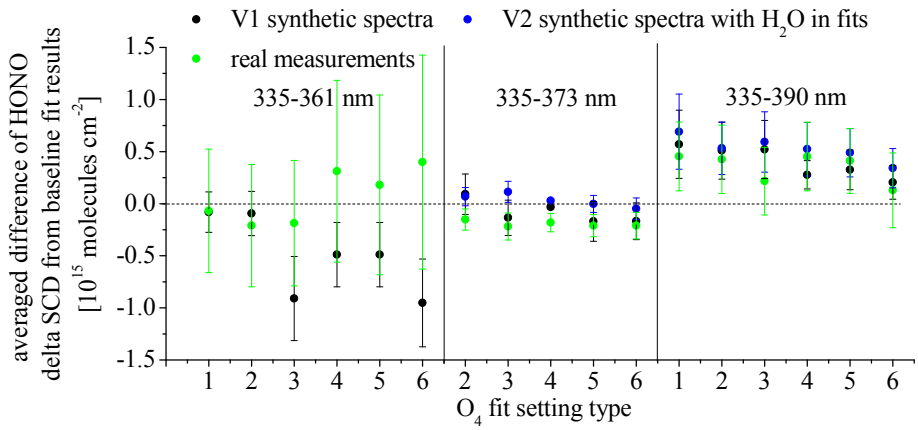

Figure S15: (a) Differences of HONO delta SCDs using six O_4 settings and three spectral ranges with respect to the real HONO delta SCDs (as used in the calculation of the synthetic spectra). (b) similar as (a), but the differences are calculated with respect to the baseline settings (O_4 setting #1 in 335-373nm). Here, in addition to the results of the synthetic spectra, also the results of the selected measurements are included. The error bars indicate the standard deviations; the numbers at the x-axes indicate the O_4 settings, see Table 4 in the main manuscript.

(a)

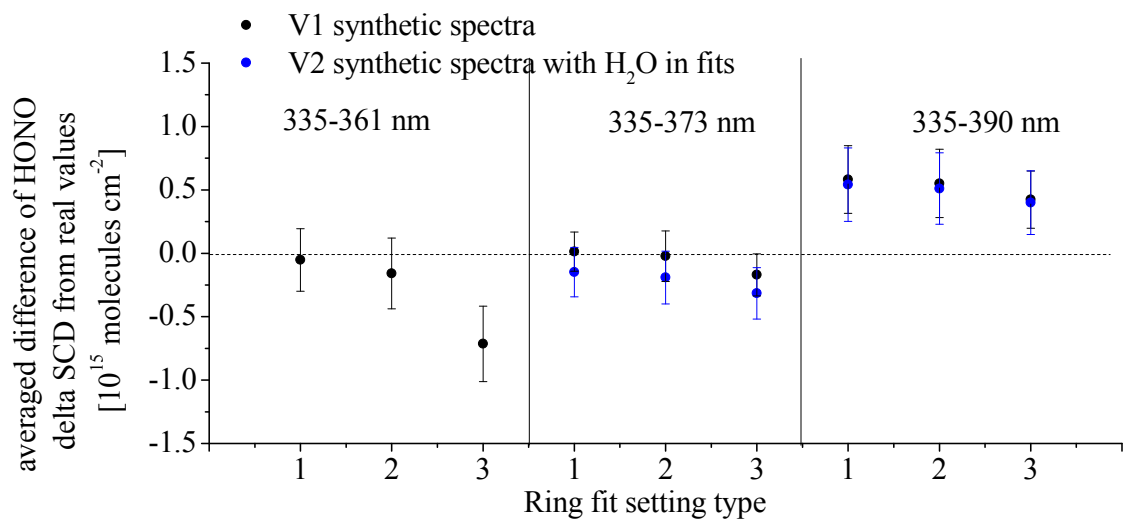

(b)

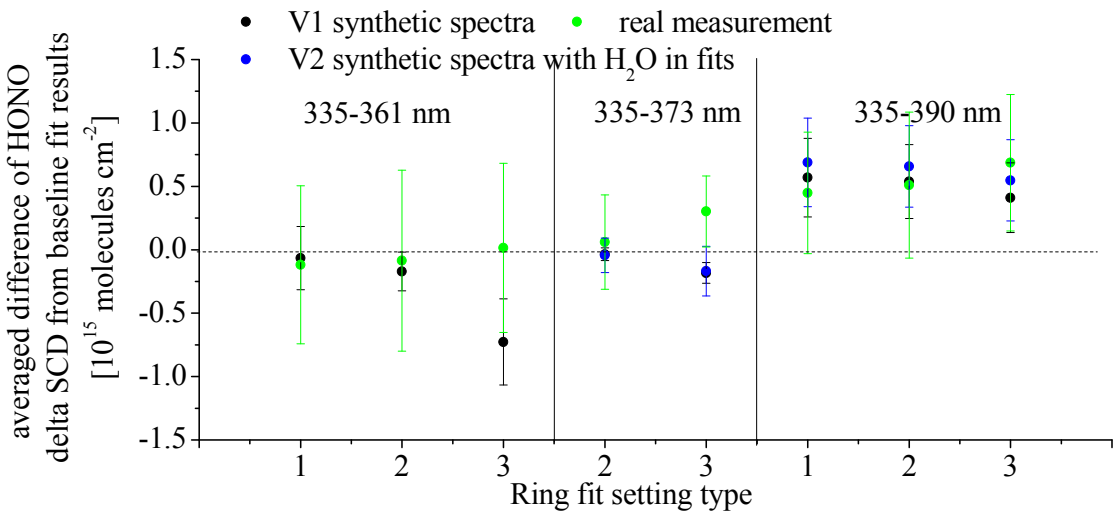

Figure S16: similar as Fig. S15, but for three different settings of the temperature dependence of the Ring effect (see Table 4 in the main manuscript).

(a)

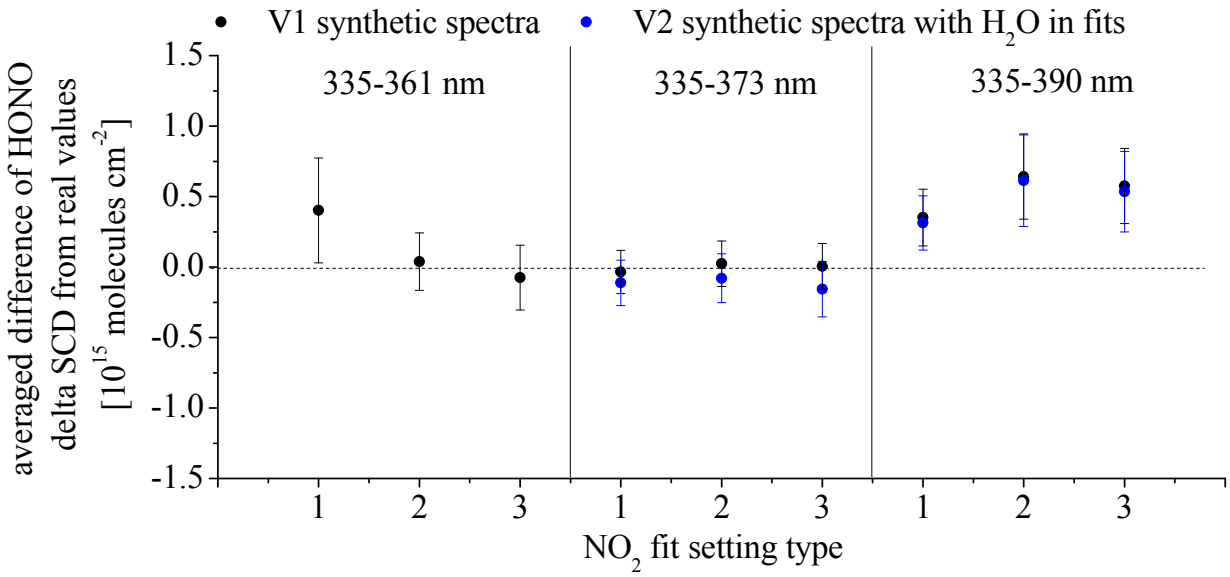

(b)

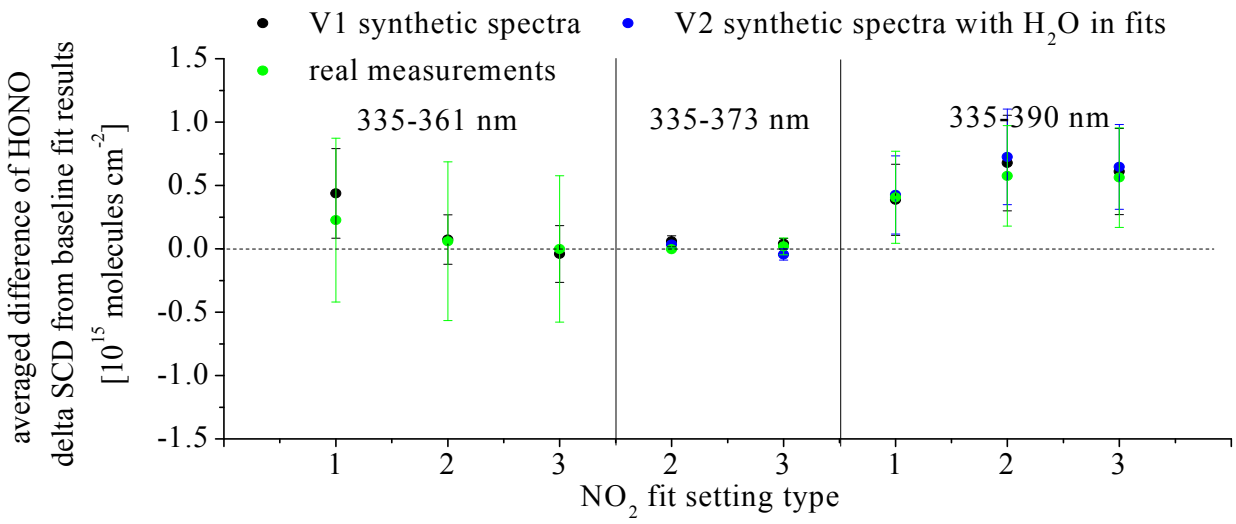

Figure S17: similar as Fig. S15, but for including different NO_2 cross sections (see Table 4 in the main manuscript).

(a)

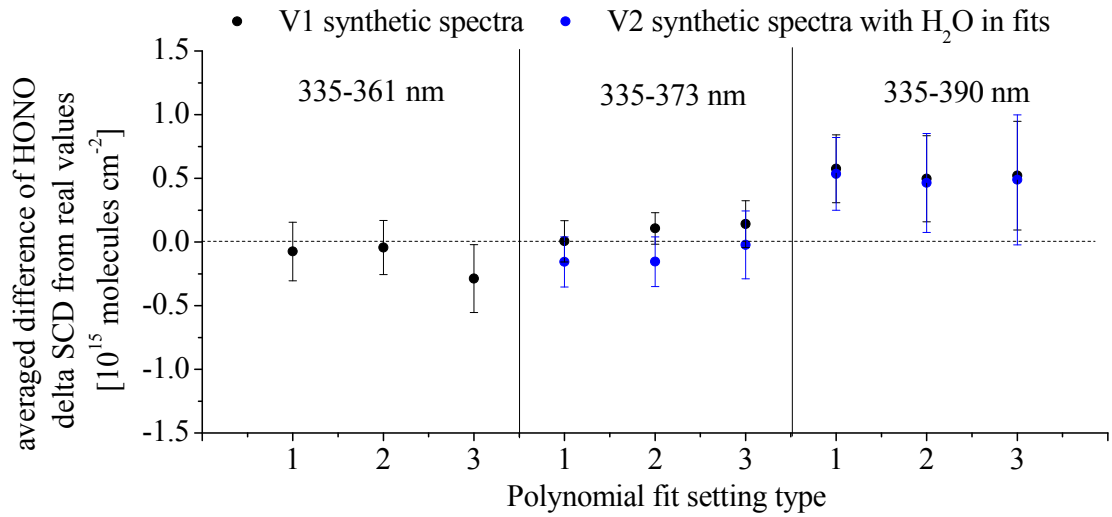

(b)

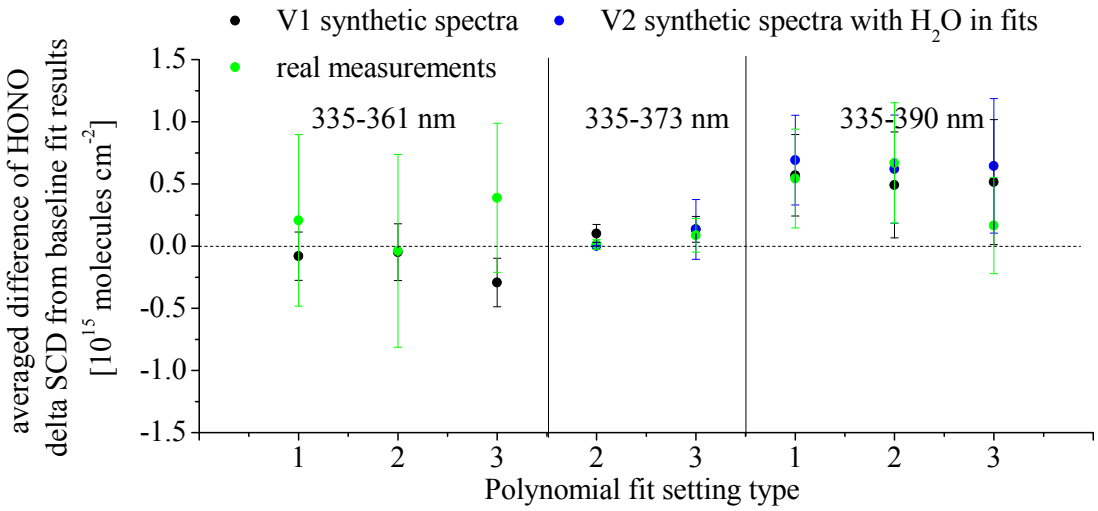

Figure S18: similar as Fig. S15, but for the different degrees of the Polynomial (see Table 4 in the main manuscript).

(a)

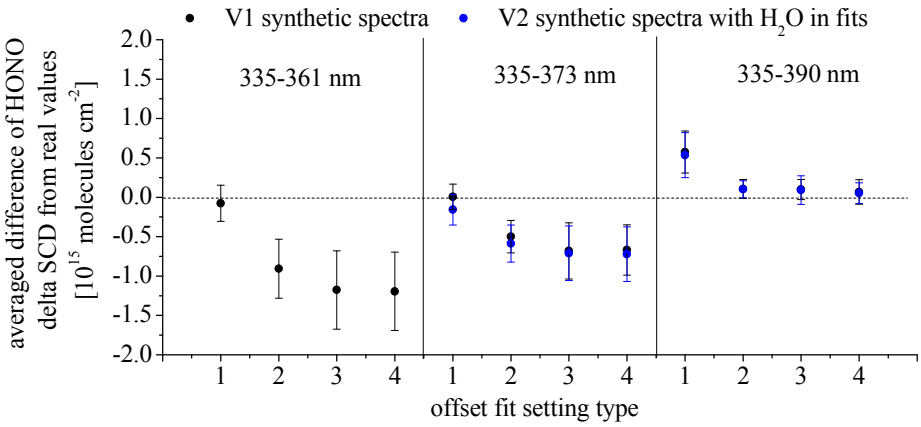

(b)

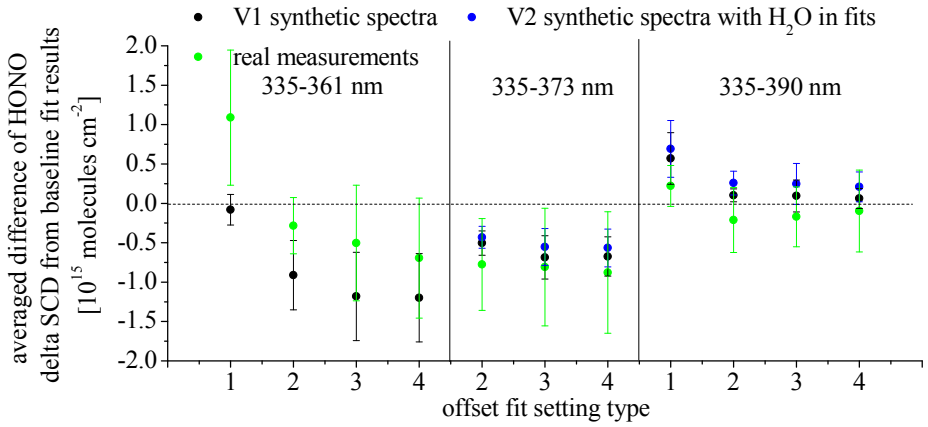

Figure S19: Similar as Fig. S15, but for the different settings of intensity offset (see Table 4 in the main manuscript).

References:

Baidar, S., Oetjen, H., Coburn, S., Dix, B., Ortega, I., Sinreich, R., and Volkamer, R.: The CU Airborne MAX-DOAS instrument: vertical profiling of aerosol extinction and trace gases, Atmos. Meas. Tech., 6, 719-739, doi:10.5194/amt-6-719-2013, 2013.

Gorshelev, V., Serdyuchenko, A., Weber, M., Chehade, W., and Burrows, J. P.: High spectral resolution ozone absorption cross-sections – Part 1: Measurements, data analysis and comparison with previous measurements around 293 K, Atmos. Meas. Tech., 7, 609-624, doi:10.5194/amt-7-609-2014, 2014.

Lampel, J., Frieß, U., and Platt, U.: The impact of vibrational Raman scattering of air on DOAS measurements of atmospheric trace gases, Atmos. Meas. Tech., 8, 3767-3787, doi:10.5194/amt-8-3767-2015, 2015.

Serdyuchenko, A., Gorshelev, V., Weber, M., Chehade, W., and Burrows, J. P.: High spectral resolution ozone absorption cross-sections – Part 2: Temperature dependence, Atmos. Meas. Tech., 7, 625-636, doi:10.5194/amt-7-625-2014, 2014.

Sinnhuber, B.M., Weber, M., Amankwah, A. and Burrows, J.P.: Total ozone during the unusual Antarctic winter of 2002. Geophysical research letters, 30(11), 2003.

Sinnhuber, M., Burrows, J.P., Chipperfield, M.P., Jackman, C.H., Kallenrode, M.B., Künzi, K.F. and Quack, M.: A model study of the impact of magnetic field structure on atmospheric composition during solar proton events. Geophysical research letters, 30(15), 2003.

Theys, N., Van Roozendael, M., Errera, Q., Hendrick, F., Daerden, F., Chabrillat, S., Dorf, M., Pfeilsticker, K., Rozanov, A., Lotz, W., Burrows, J. P., Lambert, J.-C., Goutail, F., Roscoe, H. K., and De Mazière, M.: A global stratospheric bromine monoxide climatology based on the BASCOE chemical transport model, Atmos. Chem. Phys., 9, 831-848, doi:10.5194/acp-9-831-2009, 2009.

Volkamer, R., Spietz, P., Burrows, J. and Platt, U.: High-resolution absorption cross-section of glyoxal in the UV–vis and IR spectral ranges. Journal of Photochemistry and Photobiology A: Chemistry, 172(1), 35-46, 2005.